Exploring the adsorption mechanisms of neurotransmitter and amino acid on Ti3C2-MXene monolayer : insights from DFT calculations

Exploring the Adsorption Mechanisms of Neurotransmitter and Amino Acid on Ti_3C_2-MXene Monolayer: Insights from DFT Calculations

Ilkay Ozdemir[a,b], Handan Arkin[c], Milorad V. Milošević[b], Johannes V. Barth[d], Ethem Aktürk[a,d,*]

[a]*Physics Department, Adnan Menderes University, Aydın, 09100, Turkey*
[b]*Department of Physics, University of Antwerp, Groenenborgerlaan 171, B-2020, Antwerp, Belgium*
[c]*Department of Physics Engineering, Faculty of Engineering, Ankara University, Tandogan, Ankara, 06100, Turkey*
[d]*Physics Department E20, Technical University of Munich (TUM), James Franck Strasse1, 85748, Garching, Munich, Germany*

Abstract

In this study, we conducted a systematic density functional theory (DFT) investigation of the interaction between Ti_3C_2-MXene monolayer and biological molecules dopamine (DA) and serine (Ser) as neurotransmitter and amino acid, respectively. Our calculations show good agreement with previous literature findings for the optimized Ti_3C_2 monolayer. We found that DA and Ser molecules bind to the Ti_3C_2 surface with adsorption energies of -2.244 eV and -3.960 eV, respectively. The adsorption of Ser resulted in the dissociation of one H atom. Electronic density of states analyses revealed little changes in the electronic properties of the Ti_3C_2-MXene monolayer upon adsorption of the biomolecules. We further investigated the interaction of DA and Ser with Ti_3C_2 monolayers featuring surface-termination with OH functional group, and Ti-vacancy. Our calculations indicate that the adsorption energies significantly decrease in the presence of surface termination, with adsorption energies of -0.097 eV and -0.330 eV for DA and Ser, respectively. Adsorption energies on the Ti-vacancy surface, on the other hand, are calculated to be -3.584 eV and -3.856 eV for DA and Ser, respectively. Our

*Corresponding author
Email address: ethem.akturk@adu.edu.tr (Ethem Aktürk)

results provide insights into the adsorption behavior of biological molecules on Ti_3C_2-MXene, demonstrating the potential of this material for biosensing and other biomedical applications. These findings highlight the importance of surface modifications in the development of functional materials and devices based on Ti_3C_2-MXene, and pave the way for future investigations into the use of 2D materials for biomedical applications.

Keywords: MXene, 2D Materials, Density Functional Theory (DFT), Dopamine, Serine, Biosensing, Biomedical Applications

---

1. Introduction

In 2011, owing to the demonstration by Naguib et al. [1] that two-dimensional (2D) transition metal carbide/nitride structures can be synthesized from their 3D counterparts, MAX phases, by chemical exfoliation method, the world of 2D materials has gained a novel *2D-material-family* with unique and intriguing physical properties: **MXenes**. In the MAX structures, in general, M, A and X respectively represent a transition metal, an A-group element and carbon/nitrogen. The nomenclature of the MAX phases, which was introduced with the discovery of Ti_4AlN_3 by Barsoum et al. in 2000, is now known as "$M_{n+1}AX_nphases$" where n equals 1, 2, or 3 [2, 3, 4]. MXenes are typically produced by selectively etching the A-layer from MAX phases using strong etching solutions [5]. This process leaves behind layers in the form of $M_{n+1}X_nT_x$, and the single-layer material is called MXene [1]. The name MXene reflects both the relationship with MAX phases and the structural resemblance to graphene. Here, T_x refers to surface-terminating functional groups that cover the surface during the MXene synthesis process and generally appear in the form of $T = OH, O, F$ [5]. The chemical versatility of MXene structures, both in their structural compositions (M and X regions) and surface terminations (T_x), gives rise to unique physical and chemical properties and allows for targeted adjustments to these properties for specific applications. These features have made MXene structures important in solid-state physics and materials science, and have generated significant interest in them [6, 7]. Accordingly, more than 30 MXene structures have been experimentally synthesized to date [5, 8], and over 70 have been predicted theoretically [8, 9]. Since their discovery, MXenes have garnered significant attention from physicists and chemists and shown promise for a variety of applications, including energy storage (e.g. Li/Na ion bat-

teries, supercapacitors) [10, 11, 12], photocatalysis [13, 14, 15, 16, 17], water purification [18], gas sensors [19, 20], transparent conducting electrodes [21], neural electrodes [22], photonic diodes [23], and electrochromic devices [24].

MXene structures constitute a large family of 2D materials that uniquely combine the metallic conductivity resulting from the transition metal atoms they contain and the hydrophilicity they exhibit in the presence of functional groups such as hydroxyl (OH) or oxygen (O) on their surface [25, 26]. Furthermore, MXenes are known to possess high biocompatibility [27]. These are not only their most interesting characteristics, but what make them promising materials in biomedical and nanomedicine applications, for which Ti-based MXenes ($Ti_{n+1}C_n$) are known to be the most attractive as titanium is the most biocompatible transition metal [28, 29]. Additionally, the highly sensitive response of MXene structures to electrochemical degradation makes them excellent candidates for biosensing applications [30]. For instance, Wu et al. [31] immobilized the tyrosinase-enzyme on the Ti_3C_2-MXene surface and measured the electrochemical performance of the MXene-based tyrosinase biosensor to produce a mediator-free biosensor for ultrasensitive and rapid detection of the phenol. They reported that the mediator-free biosensor based on Ti_3C_2 provides a simple, sensitive, rapid, and cost-effective method for detecting phenol in water samples, and thus Ti_3C_2-MXene may be a promising candidate for biomedical detection. Chen et al. [32] investigated the interaction mechanism between $Ti_3C_2T_x$-MXene and the simplest amino acid, glycine, both theoretically and experimentally. Their results showed that the chemical bonding of glycine on the $Ti_3C_2O_2$ surface led to an expansion of the interlayer spacing compared to the pristine surface, resulting in improved ion accessibility, enhanced charging rate, and better cycling performance. The Au/MXene nanocomposite structure as a biosensor platform was developed by Rakhi et al. [33] for enzymatic glucose sensing. Anchoring Au nanoparticles on the surface of $Ti_3C_2T_x$-MXene nanosheets improved the electrical conductivity and made the resultant Au/MXene composite a better electrochemical transducer/enzyme immobilization matrix. And the biosensors fabricated in that study exhibited significantly improved sensing performance, comparable to some of the previously reported glucose biosensors. Recently, Xu et al. developed a highly sensitive biosensing device based on Ti_3C_2-MXene-FET to detect dopamine for real-time probing neural activities [30]. According to their report, their MXene sensor could detect the dopamine at a concentration as low as 100×10^{-9} M. These and many similar studies show that MXene materials, Ti_3C_2 in particular, have significant

potential in the fields of biomedical and nanomedicine applications [27, 34] as a biosensing device.

Dopamine (DA) is an important molecule that functions as a neurotransmitter in the brain. It plays several vital roles in various physiological processes in cells, such as neural signaling, reward processes in the brain, and vasodilation outside the brain [35]. Dysfunctions or abnormal levels of the dopamine system are associated with several important nervous system disorders, including Parkinson's disease, attention deficit hyperactivity disorder, Alzheimer's disease, schizophrenia, or pheochromocytoma [36, 37, 38]. On the other hand, serine (Ser) is an α-amino acid that the human body can synthesize under normal physiological circumstances, making it nonessential [39]. Serine plays a crucial role in metabolism as it participates in the biosynthesis of numerous vital biological compounds, such as purines, pyrimidines, proteins, as well as several amino acids including glycine, and cystine. It is therefore important to develop new sensors to detect these molecules through biocompatible materials.

In this study, we investigate the interaction between Ti_3C_2-MXene monolayer (one of the most widely studied MXenes in biomedical applications, as exemplified above) and small biological molecules such as dopamine (a neurotransmitter) and serine (an amino acid). Our objective is basically to seek answers to the following questions: **(i)** Are the interactions between these biological molecules and the Ti_3C_2 monolayer strong enough to enable attachment to the surface? In other words, can these molecules be detected with Ti_3C_2-MXene monolayer? **(ii)** Can the binding of adsorbed molecules be enhanced by modifying the surface chemistry of Ti_3C_2? **(iii)** How do selected molecules affect the electronic properties of Ti_3C_2? Ultimately, identifying the details of these interactions is expected to lead to the discovery of *"intelligent surfaces"* that can function as biosensing devices in various biomedical applications.

2. Computational Methods

All of our results were obtained from first-principles plane-wave calculations based on spin-polarized density functional theory (DFT). We used projected augmented wave (PAW) potentials [40, 41] to describe the ion-electron interactions. The exchange-correlation potential was approximated by the generalized gradient approximation (GGA), using the Perdew-Burke-Ernzerhof (PBE) parametrization [42]. All theoretical analyses were per-

formed using the Vienna Ab initio Simulation Package (VASP) software [43, 44]. We included van der Waals (vdW) corrections using Grimme's DFT-D2 method [45]. To solve the Kohn-Sham equations, we used a plane-wave basis set with a kinetic energy cutoff of $\hbar^2(\mathbf{k}+\mathbf{G})^2/2m = 600\,\text{eV}$. The Brillouin zone was sampled by $(18 \times 18 \times 1)$ and $(3 \times 3 \times 1)$ special mesh points in $\mathbf{k}$-space by using Monkhorst-Pack scheme [46] for (1×1) and (6×6) cells of Ti_3C_2, respectively. All atomic positions and lattice constants were optimized by using the conjugate-gradient algorithm [47, 48] where the total energy and forces are minimized. We chose convergence criteria for the energy of $10^{-5}\,\text{eV}$ between two consecutive steps. Upon ionic relaxation, the maximum Hellmann-Feynman forces acting on each atom were less than $0.01\,\text{eV/Å}$. The maximum pressure on the unit cell was less than 1 kbar. We used the Gaussian type Fermi-level smearing method with a smearing width of 0.01 eV. Additionally, we applied the Heyd-Scuseria-Ernzerhorf hybrid functional method (HSE06) [49] to obtain corrected band values. We took the screening length of HSE06 as 0.2 Å and set the mixing rate of the Hartree-Fock exchange potential to 0.25. Finally, for charge-transfer analysis, we used the Bader analysis [50] on a charge density grid.

We calculated the cohesive energy per atom using the formula given below:

$$E_{coh} = \frac{(n_{Ti} \times E_{Ti}) + (n_C \times E_C) - E_{Ti_3C_2}}{n_{Ti} + n_C} \tag{1}$$

Here, E_{Ti}, E_C, and $E_{Ti_3C_2}$ are the total energies of the corresponding free atoms and the Ti_3C_2 monolayer, respectively. n_{Ti}, n_C indicates the total number of corresponding atoms within the structure.

The adsorption energies of selected biological molecules on the Ti_3C_2 monolayer were calculated by the following equation:

$$E_{ads} = E_{tot} - (E_{Ti_3C_2} + E_{mol}) \tag{2}$$

where E_{tot}, $E_{Ti_3C_2}$, and E_{mol} are the total energies of the Ti_3C_2+molecule system, the Ti_3C_2 substrate, and the corresponding biological molecules, respectively. In this formulation, a negative value for E_{ads} indicates that the adsorption of a molecule is favorable, and the more negative the E_{ads}, the more stable adsorption among all configurations.

The charge on the molecules, ρ_M, was calculated using Bader charge analysis [50]. Isosurfaces of the bonding charge density difference were compiled with the following expression:

$$\Delta\rho = \rho_{tot} - (\rho_{Ti_3C_2} + \rho_{mol}) \tag{3}$$

Here, ρ_{tot} is the charge of the total system, while $\rho_{Ti_3C_2}$ and ρ_{mol} are the charges of the Ti_3C_2 substrate and corresponding biological molecules, respectively.

We generated charge density plots and visualized all structures using the VESTA program [51]. For the calculation of the phonon modes within a (3×3) supercell, we used the PHONOPY code [52], which is based on the density functional perturbation theory (DFPT) of the plane-wave method. To account for localized hybridization in the *d*-orbitals of the Ti atom, we included the Hubbard U (GGA+U) correction in the calculations. We used a correction term of $U = 4.20\ eV$, whose efficiency was already proven semi-empirically in a previous study [53]. We included this correction for comparison purposes in the monolayer limit.

We calculated the work function W by the difference [54]

$$W = -e\phi - E_F \tag{4}$$

where $-e$ represents the charge of an electron, ϕ denotes the electrostatic potential in the vacuum nearby the surface, and E_F is the Fermi level, which corresponds to the electrochemical potential of electrons within the material. The term $-e\phi$ represents the energy of a stationary electron in the vacuum nearby the surface.

3. Results and Discussion

The main objective of this study is to investigate, at the atomic level, the interaction between Ti_3C_2-MXene monolayer and selected biological molecules, namely dopamine (DA) as a neurotransmitter and serine (Ser) as an amino acid, using first-principles density functional theory calculations. We begin by exploring the properties of the Ti_3C_2 monolayer in the unit cell, followed by the creation of a (6×6) supercell to analyze the interaction between the supercell and the selected biological molecules. Geometric optimizations were performed with high precision, and the effects on the structural and electronic properties were analyzed and discussed. The findings obtained within the scope of the present study are organized under the relevant subheadings below.

3.1. Structural and Electronic Characteristics of Ti_3C_2 Monolayer

As illustrated in Fig.1(a), a single Ti_3C_2 laminate consists of five atomic layers stacked in the sequence Ti(1)-C(1)-Ti(3)-C(2)-Ti(2) from bottom-to-top, exhibiting a hexagonal structure within the *P3m1* space group. In the

structure, each C atomic layer is sandwiched between two Ti atomic layers. Besides, each Ti atom on the surface bonds with the three nearest C atoms, while the Ti atoms in the intermediate layer bond with the six C atoms nearest to them. As for the C atoms, each bonds with six Ti atoms. After optimizing the structure, two different bond lengths between Ti atoms and C atoms have been obtained, that is, d_1 is the bond between Ti(1) and C(1) or Ti(2) and C(2), while d_2 is the bond between Ti(3) and C(1) or Ti(3) and C(2). (See Fig.1(a), side view) The bond lengths calculated without and with Hubbard parameter as well as corresponding relevant structural parameters such as lattice constants, thickness, cohesive energy, charge transfer, magnetic moment are listed in Table 1.

Table 1: Structural parameters calculated without and with Hubbard parameter (w/o U and w U, respectively) for Ti_3C_2 monolayer: The lattice constants, in the (xy)-plane $|\vec{a}|=|\vec{b}|$=a, and along the z direction (vacuum), $|\vec{c}|$=c; the thickness parameter, Δz; the bond lengths between neighboring Ti and C atoms, d_1 (Ti(1)-C(1) and Ti(2)-C(2)), d_2 (Ti(3)-C(1) and Ti(3)-C(2)); cohesive energy per atom, E_{coh}; the average electronic charge transfer from Ti atoms to C atoms obtained from Bader charge analysis, $\Delta\rho$; the magnetic moment in the unit cell and on Ti atoms residing at the surface, μ_B.

Hubbard	lattice constants		thickness parameter	bond lengths		cohesive energy	charge transfer	magnetic moment μ (μ_B)	
(U=4.2 eV)	a (Å)	c (Å)	Δz (Å)	d_1 (Å)	d_2 (Å)	E_{coh} (eV/atom)	$\Delta\rho$ (e)	unit cell	on Ti
w/o U	3.097	20	4.677	2.067	2.212	6.98	1.16	–	0.761
w U	3.147	20	4.922	2.145	2.246	5.07	1.26	–	1.297

In order to verify the accuracy and reliability of our first-principles-based calculations and the parameters employed, we conducted phonon dispersion curve calculations along the main symmetry directions across the Brillouin zone. The stability of the Ti_3C_2 monolayer is crucial to validate the feasibility of our calculations as it is an experimentally synthesized material. As depicted in Fig.S1 in the Supplementary Material (SM) [55], the positive phonon frequencies and the calculated cohesive energy, which signifies strong bonding within the structure, demonstrate the stability of the Ti_3C_2 monolayer. Additionally, we compared our calculated phonon dispersion spectra with those reported in the theoretical literature and found them to be in good agreement, further supporting the accuracy of our calculations and parameters.

Once we are sure of the accuracy and reliability of our calculations by obtaining the Ti_3C_2 as a stable monolayer, we proceeded to investigate its electronic properties. Isosurfaces of the charge density difference ($\Delta\rho(\mathbf{r})$)

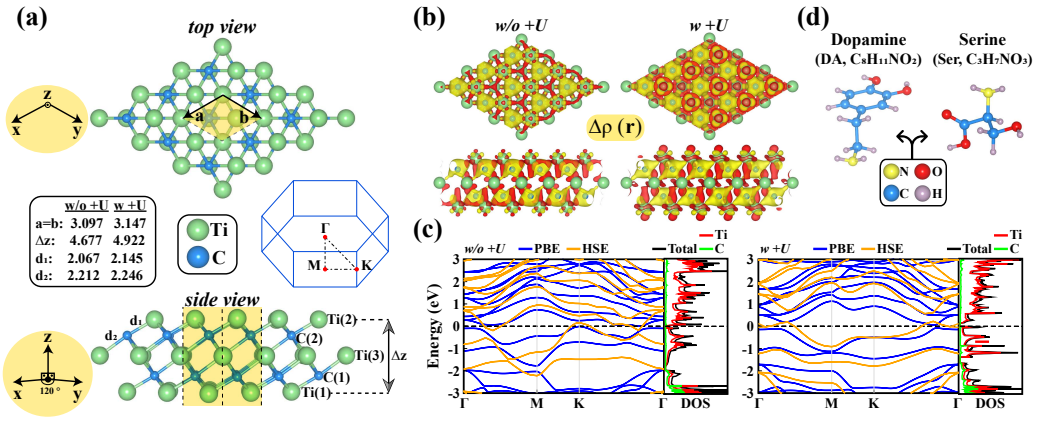

Figure 1: **(a)** Optimized atomic configuration of Ti_3C_2 monolayer from top and side views. The 2D unit cell is highlighted within the yellow shaded area and relevant structural parameters (without (w/o) and with (w) Hubbard-U parameter where U=4.2 eV/Ti) are indicated. The corresponding hexagonal Brillouin zone is also given inset with the main symmetry directions. **(b)** Isosurfaces of the charge density difference, $\Delta\rho(\mathbf{r})$, for Ti_3C_2 monolayer, calculated without and with Hubbard parameter. The yellow and red isosurfaces represent positive and negative electron densities, respectively. **(c)** Electronic energy band structures calculated within PBE and HSE along the main symmetry directions in the Brillouin zone, without and with Hubbard parameter, along with the corresponding density of states of Ti_3C_2 monolayer. The Fermi energy is set to zero and shown by a black-dashed line. **(d)** Optimized atomic structures of the selected biological molecules, dopamine and serine, with the abbreviation and general chemical formula for each molecule indicated.

in Fig.1(b), obtained by subtracting the free atom charge densities from the total charge density of Ti_3C_2 monolayer, reveal the charge transfer characteristics and chemical bonding mechanism between Ti and C atoms. As shown in the figure, there is considerable electronic charge transfer from Ti atoms to C atoms. According to Bader [50] charge analysis, while the electronic charge transfer calculated without (with) Hubbard parameter from Ti atoms on the surface to C atoms is 1.04 (1.09) e, it is 1.42 (1.60) e from Ti atoms in the intermediate layer to C atoms. Thus, an average charge transfer of 1.16 (1.26) e/Ti (or 1.75 e/C (1.89 e/C)) from Ti atoms to C atoms took place. Additionally, hybridized electrons localized in the 3d-orbitals of Ti atoms (especially for the Ti atoms located at the surfaces) are visible in the charge density isosurfaces calculated with Hubbard interaction. These hybridized electrons have an impact on the electronic energy bands of Ti_3C_2 monolayer. From the left panel of Fig.1(c), Ti_3C_2 appears to be a metallic

structure, whereas a small indirect gap (0.13 eV) has occurred due to the effect of the Hubbard interaction. However, this gap is closed by the HSE correction [49], a hybrid functional known to more accurately estimate the bandgap, leading to the conclusion that Ti_3C_2 monolayer has a metallic characteristic. In both cases, the main contribution to the electronic structure around the Fermi level comes from $3d$-orbitals of Ti atoms as can be seen from the electronic density of states in Fig.1(c).

Furthermore, we investigated the ground state of Ti_3C_2 monolayer in terms of magnetism, comparing anti-ferromagnetic (AFM) and ferromagnetic (FM) states. In the AFM structure, we assumed that the atoms on the same surface are ferromagnetically arranged, while the atoms on different surfaces have opposite spin ordering. In the FM structure, all Ti atoms on the surfaces are aligned in the same spin orientation. Ti atoms in the intermediate layer and C atoms are nonmagnetic. The configurations and corresponding total energies calculated by DFT are described in the SM [55] (see Fig.S2), and it is concluded that Ti_3C_2 monolayer has an AFM ground state. This anti-ferromagnetic metallic nature of Ti_3C_2 has been previously reported in the literature [56, 57, 58].

3.2. Selected Molecules

As previously mentioned, dopamine (DA) was selected as the neurotransmitter molecule and serine (Ser) as the amino acid in this study. Before investigating the interaction of these molecules with the Ti_3C_2 monolayer, their structural properties were optimized and analyzed, as shown in Fig.1(d). In addition, we calculated optimized bond lengths, cohesive energy, electronic energy diagrams, and HOMO-LUMO energy gap (HLG) values, which were presented in the Supplementary Material [55] along with literature comparisons. Furthermore, we provided a brief explanation of why these molecules were chosen for this study, highlighting some of their important functions in the body, as follows:

- **Dopamine (DA)**, with a chemical formula of $C_6H_3(OH)_2$-CH_2-CH_2-NH_2 or $C_8H_{11}NO_2$, belongs to the catecholamine family of neurotransmitters in the brain and serves as a precursor to epinephrine (adrenaline) and norepinephrine (noradrenaline). It is a chemical that can be naturally produced in the body and functions as both a hormone and a neurotransmitter, playing many essential roles in the brain and body

[59, 60, 61, 62]. In the brain, it acts as a neurotransmitter by activating dopamine receptors. In the blood vessels, it inhibits the release of norepinephrine and acts as a vasodilator at normal concentrations; increases sodium excretion and urine output in the kidneys; reduces insulin production in the pancreas; reduces gastrointestinal motility in the digestive tract and protects the intestinal mucosa; and in the immune system, it reduces the activity of lymphocytes. Parkinson's disease, known as a degenerative condition that causes tremors and motor impairment, is caused by the loss of dopamine-secreting neurons in the area called black substance (*substantia nigra*) in the midbrain. There is evidence of varying levels of dopamine activity in schizophrenia, and most antipsychotic drugs used in its treatment are dopamine antagonists that reduce dopamine activity [63]. Attention deficit hyperactivity disorder (ADHD), restless legs syndrome, bipolar disorder, and addiction are also characterized by dopamine production or defects in metabolism [64].

In addition, dopamine is known for its superior biocompatibility properties in the field of biomaterials as well as its excellent adsorption ability [65]. All these findings suggest that developing new sensors to detect dopamine is of great important.

- **Serine (Ser, $C_3H_7NO_3$)** is an amino acid essential for protein biosynthesis and metabolism. It is involved in the production of purines and pyrimidines, and serves as a key component in the catalytic function of numerous enzymes. Additionally, serine plays a vital role in intercellular communication between nerve cells, particularly in the form of D-Serine [66].

Adsorption of DA and Ser molecules onto Ti_3C_2-MXene has practical applications in the fields of biosensing, biofilm development and bioimaging, and theoretical studies, which are the first steps in this field, are very valuable for experimenters [67]. Selective and highly sensitive biosensors can be developed by examining the adsorption behaviors of DA and Ser molecules by utilizing different surface modifications. In other words, the degree of interaction of the Ti_3C_2-MXene surface with molecules and the electrical and magnetic properties of the surface can be changed by modification of surface groups or by creating vacancies on the surface. This implies that developing biosensors and other devices based on Ti_3C_2-MXene materials will require

an understanding of the interactions between the biomolecules and the bare monolayer and its modified counterparts [68, 69].

3.3. Interaction of Ti_3C_2 Monolayer with Biological Molecules

As a first step, to determine the most stable adsorption configuration of each selected biological molecule on the Ti_3C_2 monolayer, we performed single-step self-consistent (SC) calculations with several initial orientations and adsorption sites. The configurations were created by determining the different possibilities that the biomolecules DA and Ser could approach the surface, taking into account the geometry of the molecules and the topology of the surface. Consideration of these several configurations can be described as follows: **(i)** DA can be adsorbed on the surface through four distinct sites; the NH_2 end, two distinct OH ends, and in parallel orientation to the surface. **(ii)** Similarly, Ser can adopt four different adsorption sites, that is, through the NH_2 end, two distinct OH ends, and the O end. (See Fig. 1(d)) All these configurations were systematically explored on various locations of the Ti_3C_2 surface. The total energy values obtained through these SC calculations are graphically presented in Fig.2. The two configurations with the lowest energy for each structure were fully optimized to obtain precise ground-state structures. The optimized structures with the minimum energy among these duals were determined as the most stable adsorption configurations for the respective systems.

Calculated minimum-energy configurations for each molecule on Ti_3C_2 monolayer are shown in Fig.2. As can be seen from the figure, after the optimization process, no significant deformation occurred in the atomic structure of the Ti_3C_2 monolayer in both systems. As for the molecules, it is seen that one of the hydrogen atoms in the serine dissociated, while only small fluctuations occurred in the dopamine. The most stable configuration of the DA molecule on the Ti_3C_2 surface was obtained to have the benzene ring and two hydroxyl groups in the horizontal position above the surface and the amine group away from the surface. For Ser, on the other hand, it can be seen that the oxygen atom in the side chain of the Ser was attached to the surface, and the hydrogen atom initially attached to this oxygen dissociated from the Ser. Both DA and Ser preferred to adsorb on the Ti_3C_2 monolayer via their oxygen sites. The calculated bond lengths between Ti-O atoms are 2.15 Å and 2.18 Å for the Ti_3C_2+DA and Ti_3C_2+Ser systems, respectively. The hydrogen atom dissociated from the Ser has three nearest Ti atoms with a distance of 2.04 Å. We calculated the adsorption energies on Ti_3C_2 substrate

as −2.244 eV for DA and −3.960 eV for Ser by using Equation(2). These negative adsorption energies indicate that the adsorption mechanisms are thermodynamically favorable, and that the biomolecules can spontaneously and exothermically adsorb onto the surface of Ti_3C_2-MXene monolayer, resulting in stable structures. To determine the deformation energies of the molecules, on the other hand, we subtracted the energy of the optimized isolated molecules from the energy of the molecule in the geometry of Ti_3C_2+M complex system: $E_{def} = E_{mol}^{complex} - E_{mol}^{isolated}$. Our calculations yielded deformation energies of 2.479 eV for DA and 5.900 eV for Ser. The respective deformation energies are positive as the molecules have a well-defined equilibrium geometry corresponding to their lowest energy states and any deformation from their equilibrium geometries will require additional energy. Furthermore, since the energy of Ser involves not only sorption but also the dissociation of one hydrogen atom from the molecule, it results in a much higher deformation energy compared to that of DA. In a similar manner, the energy of the distortion of the Ti_3C_2-MXene substrate in the Ti_3C_2-DA and Ti_3C_2-Ser systems were calculated as 0.171 eV and 0.168 eV, respectively.

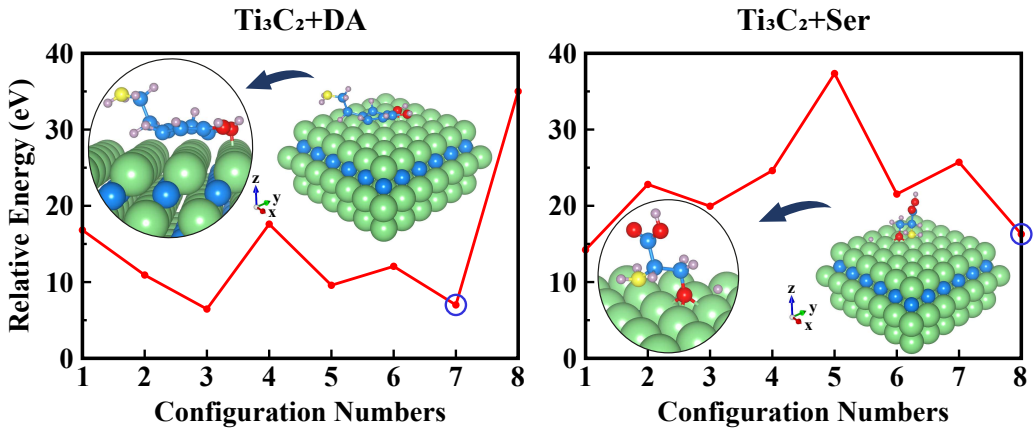

Figure 2: Ti_3C_2+Molecule systems. Relative total energy values are calculated within SC calculations for various configurations, the minimum energy of which is given in a blue circle. Fully optimized atomic structures of Ti_3C_2+DA and Ti_3C_2+Ser systems at minimum-energy configurations are also presented.

Isosurfaces of electronic charge density difference, $\Delta\rho(\mathbf{r})$, which is obtained by subtracting the charge densities situated at the Ti_3C_2 substrate and molecule sites from the charge density of the total system, and par-

tial electronic density of states (DOS) graphs were plotted to examine the effect of adsorption process on the electronic properties of the Ti_3C_2 monolayer. (See SM [55], Fig.S4) Overall, the DOS diagrams for both systems show qualitative similarities. Particularly, the surface's contribution to the total DOS in both systems bears a close resemblance to that of the pristine Ti_3C_2 monolayer. This is understandable as the weak distortion energy of the Ti_3C_2 surface in both systems results in a small perturbation of the electronic structure, which is desirable for the effective protection of the sensing surface against external influences. It is also noteworthy that the Ti_3C_2 surface, which is metallic in its pristine form, maintains its metallic state after the adsorption of molecules. With the adsorption of molecules, there was some shift in energy levels in both spin-up and spin-down polarization channels, leading to the dissymmetry of the spin-up and spin-down channels in the DOS graphs. This indicates charge flow between the surface and the molecules. Accordingly, charge density difference plots of the biological molecules adsorbed on the Ti_3C_2 surface are shown in Fig.S4 in the SM [55]. As can be seen, there is an evident charge transfer between molecules and Ti_3C_2 surface. Quantitative values of the amount of total charge on the molecules and on the Ti_3C_2 surface were estimated by Bader analysis [50] in units of electrons (e). As a result, we obtained 1.77 e and 1.41 e excess charge on DA and Ser, respectively. Concurrently, we incorporated the density-derived electrostatic and chemical method, DDEC6 [70, 71, 72], to provide a more comprehensive understanding of the charge distribution within the system under investigation. Employing the DDEC6 method yielded excess charge values of 1.09 e on DA and 1.08 e on Ser. Despite the quantitative difference between the two methodologies, both consistently demonstrated a net loss of electrons from the surface and thus affirmed that the direction of the electronic charge transfer is from the surface to the molecule. This can be detected as a decrease in current through a Ti_3C_2-based-sensor. The only exception is the hydrogen atom dissociated from the Ser, which gained 0.61 e according to Bader analysis, and is surrounded with accumulated-charged isosurfaces in Fig.S4. The charge redistribution between a metallic surface and an adsorbed molecule (adsorbate) is widely acknowledged as a factor influencing the work function, a fundamental electronic characteristic for metallic surfaces in solid-state physics. The work function represents the minimum thermodynamic energy necessary to extract an electron from a solid to a point in the vacuum sufficiently far outside the surface. Indeed, changes in the work function are typically correlated with variations in surface dipole moments stemming from

the rearrangement of electron density upon adsorption. When the adsorbed molecule exhibits greater electronegativity compared to the substrate, electron transfer from the surface to the adsorbate layer occurs, resulting in an excess of negative charges on the outside and an excess of positive charges on the inside of the surface. This leads to a negative dipole moment (oriented inward) that reinforces the inherent surface dipole due to electron "spill out", thereby leading to an increase in the work function. Conversely, a decrease in work function is expected for electropositive adsorbates. [73, 74] In this study, we conducted calculations, using Equation(4), to determine the work function of systems involving the adsorption of DA and Ser molecules onto the pristine Ti_3C_2 surface. As illustrated in Fig. S7 in the SM [55], we observed an increase in the work function on the side where molecules are adsorbed to the surface. This phenomenon is comprehensible and arises from the direction of charge transfer from the surface to the molecules, leading to the formation of a negative dipole on the Ti_3C_2 surface. Besides, as a result of these interactions, that is, the charge transfer between the surface and the molecules, and concomitant shifts in energy levels in the DOS graphs, magnitudes of the local magnetic moments on the magnetic Ti atoms in the region close to the molecule in the uppermost layer have changed, while their directions are preserved. In the end, upon adsorption of the molecules, Ti_3C_2 retains its anti-ferromagnetic metallic behavior.

Table 2: Calculated adsorption energies (E_{ads}) and deformation energies (E_{def}) (in eV) of the selected molecules on the Ti_3C_2 surface in equilibrium, with -OH termination, and under vacancy defect.

	Adsorption Energy			Deformation Energy		
	Ti_3C_2	$Ti_3C_2(OH)_2$	Ti-vacancy	Ti_3C_2	$Ti_3C_2(OH)_2$	Ti-vacancy
DA	-2.244	-0.097	-3.584	2.479	0.008	3.266
Ser	-3.960	-0.330	-3.856	5.900	0.078	2.096

3.4. Effects of Surface Termination on the Interaction Between Ti_3C_2 Monolayer and Selected BioMolecules

We also conducted an investigation into the interaction of Ti_3C_2-MXene with selected biological molecules under the influence of certain surface modifications, focusing first on surface termination. In the previous studies in literature, it has been reported that dopamine can strongly interact with

the free electrons of functional termination groups, such as hydroxyl, on the graphene surface via π-π interaction, thereby leading to a doping effect. [75, 76, 77]. Accordingly, the surface termination effect with the -OH functional group was taken into account within this study. In order to find the most favorable configuration, we employed a similar approach to the pristine Ti_3C_2 case, initially testing several orientations and adsorption sites for the molecules using single-step SC calculations. Total energy values obtained by these SC calculations are given in Fig.3. It is clear from Table 2 that the adsorption energies between the surface and the molecules significantly reduced under the surface termination effect compared to the pristine state. This may be expected from the fact that oxygen-terminated MXenes are less reactive for adsorption phenomena than their pristine counterparts [78, 29]. Additionally, through hydrogen compensation, the degree of electrostatic attraction between the O-terminated surface and the molecules might further be reduced [79]. In Fig.3, no appreciable structural deformation was observed in either the molecules or the $Ti_3C_2(OH)_2$ substrate. Both DA and Ser preferred to adsorb to the surface through the N atom in the amine group. The calculated distances between the N atom within the molecule and the Ti atom at the surface are 1.87 Å and 1.86 Å in $Ti_3C_2(OH)_2$+DA and $Ti_3C_2(OH)_2$+Ser systems, respectively.

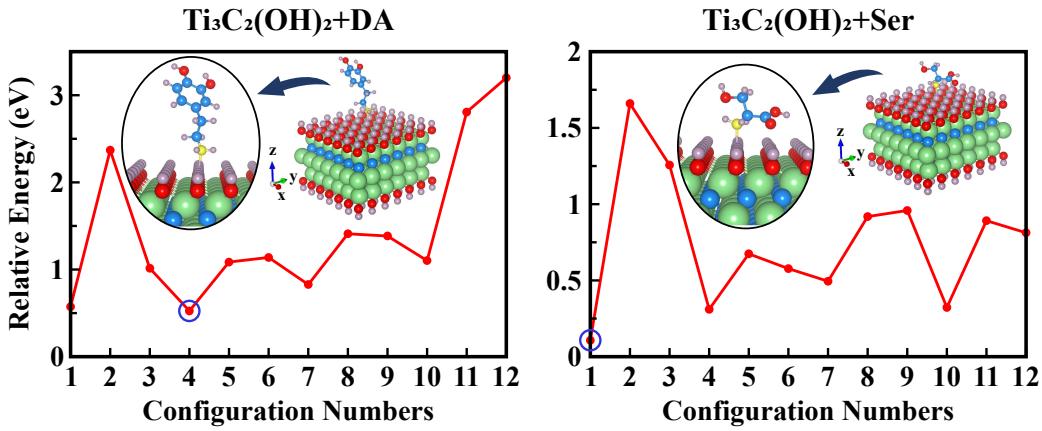

Figure 3: $Ti_3C_2(OH)_2$+Molecule systems. Relative total energy values are calculated within SC calculations for various configurations, the minimum energy of which is given in a blue circle. Fully optimized atomic structures of $Ti_3C_2(OH)_2$+DA and $Ti_3C_2(OH)_2$+Ser systems at minimum-energy configurations are also presented.

Following the optimization of the atomic structure and determination of the minimum energy configuration, we examined the electronic properties of $Ti_3C_2(OH)_2$+M (M:DA, Ser) systems. In this regard, we calculated the electronic charge density difference and electronic density of states, plots of which are given in the SM [55] Fig.S5. Using the Bader method, we determined the excess charges on DA and Ser within the $Ti_3C_2(OH)_2$+DA and $Ti_3C_2(OH)_2$+Ser systems to be 0.12 e and 0.37 e, respectively. Alternatively, employing the DDEC6 method yielded excess charge values of 0.12 e and 0.30 e on DA and Ser, respectively. Again, despite the variation in quantitative outcomes between two methodologies, both consistently indicate a transfer of charge from the surface to the adsorbed molecules.

3.5. Effects of Vacancy Defect on the Interaction Between Ti_3C_2 Monolayer and Selected BioMolecules

Lattice defects are known to have a significant impact on the fundamental properties of materials. In fact, in the case of 2D materials, the emergence of atomic-scale defects during the manufacturing process is inevitable [80]. While point defects may have negative connotations, they can actually be beneficial for specific applications by offering opportunities to modify material properties and create novel functionalities, a process known as defect engineering [81, 82]. Within this study, as another surface modification, we considered vacancy defect which is created on the surface of Ti_3C_2 monolayer by removing one Ti atom. Above this cavity formed after the removal of the atom, we placed the molecules with their minimum energy configurations obtained for the pristine case. The fully and precisely optimized atomic configurations of these systems are presented in Fig.4. Under the influence of the vacancy defect, the DA molecule maintained its parallel orientation but rotated horizontally by approximately 30°. As a result of this rotation, while one oxygen atom from DA is attached to surface Ti atoms in the pristine case, two oxygen atoms are attached to the Ti-vacancy surface. One of them is bonded with one Ti atom (O2-Ti57) and the other with two Ti atoms (O1-Ti62 and O1-Ti63). The calculated bond lengths are as follows: $d_{O2-Ti57}$=2.19 Å, $d_{O1-Ti62}$=2.32 Å and $d_{O1-Ti63}$=2.28 Å. As for Ser, its adsorption configuration changed significantly compared to the pristine case. First, there is no dissociation for H atoms. Second, Ser was interacting with the pristine Ti_3C_2 surface in a vertical orientation through its hydroxyl side. Upon the Ti-vacancy surface, on the other hand, it adsorbed to the surface parallelly and with three oxygen atoms. One of the hydrogen atoms from

Ser almost fills the cavity formed after the removal of the Ti atom from the surface. The calculated bond lengths between oxygen atoms and titanium atoms are 2.32 Å, 2.21 Å and 2.04 Å. The adsorption energies were found to be −3.584 eV and −3.856 eV for DA and Ser, respectively. Table 2 clearly shows that the adsorption energies of dopamine and serine on the Ti-vacancy surface are higher than those on the pristine surface, indicating that the presence of Ti vacancy enhances the interaction between the Ti_3C_2 monolayer and the selected biological molecules. This increase in adsorption energy was observed even in the case of Ser, despite the apparent decrease, because the dissociation of one H atom in the pristine case contributes to the adsorption energy. The increase in adsorption energy can be attributed to the fact that the Ti-vacancy introduces additional binding sites and alters the electronic structure of the Ti_3C_2 monolayer, which in turn affects the interaction with the biological molecules.

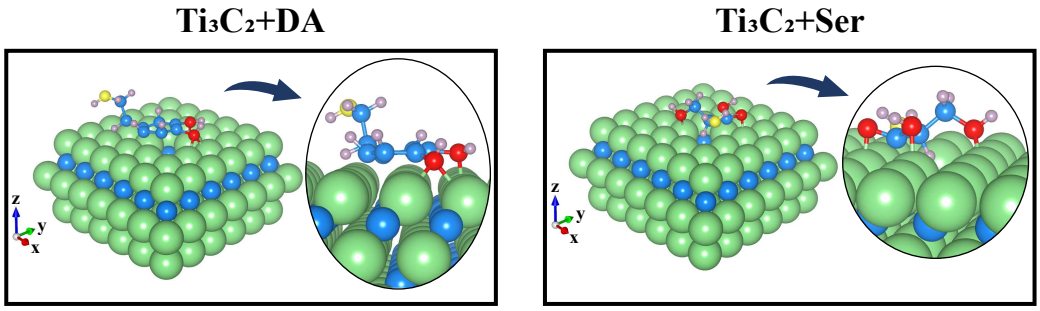

Figure 4: Optimized atomic structures of Ti_3C_2+DA and Ti_3C_2+Ser systems with Ti-vacancy surface.

To examine the electronic properties of Ti_3C_2+M systems with Ti-vacancy surface, we generated the electronic charge density difference isosurfaces and electronic density of states plots, which are given in the SM [55] Fig.S6. The calculated Bader charges on DA and Ser in the Ti_3C_2+DA and Ti_3C_2+Ser systems with Ti-vacancy surface were found to be 1.80 e and 1.11 e, respectively. With some deviations, the DDEC6 method yielded values of 1.10 e for DA and 0.65 e for Ser. Despite the quantitative difference between the methodologies, both approaches consistently reveal a directional flow of charge from the substrate to the adsorbed molecules.

The interactions of biomolecules with 2D materials alter the charges on the atoms and other properties, creating a signal that can be detected in

different ways based on the type of sensor. Charge transfer and orbital interactions, which are essential to sensing are involved in most interactions. By the Bader charge analysis or DDEC6 charge analysis the charges on the atoms can be computed and hence shows the flow of charge from the MXene substrates to the biomolecules which cause to sense the biomolecules by the MXene substrates. More specifically, the first step in sensor design is to create a signal from a measurable physical or chemical quantity that exists between the sensor surface and the molecule that needs to be detected, or recognized. This signal is produced by charge transfer that occurs during adsorption in an electrochemical sensor. The creation of effective biosensors may benefit greatly from theoretical simulations, which can shed light on a variety of topics including charge transfer, adsorption energy, and the interaction of biomolecules on 2D materials. This makes it possible for theoretical models to forecast whether a material will be suitable for a sensing application, which helps direct the execution of laboratory research. Another useful value for sensing applications could be the alteration in the work function of the material. In our study, the change in work functions were also considered. The design of sensors also benefits from this distinction.

4. Conclusion

In conclusion, our theoretical study explored the adsorption of biological molecules on Ti_3C_2-MXene surface, utilizing pristine, OH-terminated, and Ti-vacancy surfaces. Based on the first-principles plane-wave calculations within DFT performed on the Ti_3C_2-MXene monolayer, it was found that the optimized structure of the monolayer exhibits anti-ferromagnetic metallic characteristics, consistent with previous literature results. Further investigations carried out on the interaction between the Ti_3C_2 monolayer and the biological molecules dopamine (DA) and serine (Ser) indicated that there was a dissociation of one of the hydrogen atoms in the serine molecule, while small fluctuations occurred in the dopamine molecule. The results suggest that DA and Ser molecules can spontaneously and exothermically adsorb on the surface of Ti_3C_2-MXene monolayer, with Ser showing higher affinity for the surface due to its stronger interaction.

Moreover, we thoroughly examined the interaction of the same biological molecules with Ti_3C_2 monolayer featuring surface-termination with OH functional group and Ti_3C_2 monolayer with Ti-vacancy, providing crucial insights into the intricate interplay between surface modifications and adsorption be-

havior of Ti_3C_2-MXene towards these molecules. Our results showed that the presence of the OH-termination on the Ti_3C_2 monolayer surface led to a significant decrease in the adsorption energy of dopamine and serine molecules, indicating weaker binding. On the other hand, the Ti-vacancy in the Ti_3C_2 monolayer increased the adsorption energy of these molecules, suggesting stronger binding.

The results of this study have implementations on the applications of the Ti_3C_2-MXene surface in biomedical technologies such as biosensors, biofilms, and coating materials by controlling the interaction of the Ti_3C_2-MXene surface with biological molecules DA and Ser. Revealing the interaction of biological molecules with surfaces, which is considered theoretically in this field, has a very important place in the development of technologies such as biosensors. Our key finding is that, in case the Ti_3C_2-MXene surface is modified with the OH-functional group, DA and Ser molecules bind very weakly to the surface, and this weak binding interaction may find application in the biomedical field, such as biofilm production on the surface, thus preventing bacterial aggregation and surface corrosion. As another showcase, when Ti-vacancy is introduced on the Ti_3C_2-MXene surface, and the interaction of the surface with DA and Ser molecules increases considerably. This strong bonding can be crucial for bio-imaging such as magnetic resonance as a contrast agent and may guide experimentalists.

5. Acknowledgments

This work is supported by TUBITAK under Project No. 118F508. IO thanks to the Council of Higher Education (the CoHE) 100/2000 Program and to the Scientific and Technological Research Council of Turkey (TUBITAK) BIDEB-2214/A Program for providing doctoral scholarships. E. A. acknowledges the Alexander von Humboldt Foundation for a Research Fellowship for Experienced Researchers. The computational resources are provided by TÜBITAK ULAKBIM, High Performance and Grid Computing Center (TR-Grid e-Infrastructure), the Leibniz Supercomputing Centre.

References

[1] M. Naguib, M. Kurtoglu, V. Presser, J. Lu, J. Niu, M. Heon, L. Hultman, Y. Gogotsi, M. W. Barsoum, Two-dimensional nanocrystals produced by exfoliation of ti3alc2, Advanced Materials 23 (2011) 4248–4253. doi:10.1002/adma.201102306.

[2] M. W. Barsoum, The mn+1axn phases: A new class of solids: Thermodynamically stable nanolaminates, Progress in Solid State Chemistry 28 (2000) 201–281. doi:10.1016/S0079-6786(00)00006-6.

[3] M. W. Barsoum, T. El-Raghy, A. Procopio, Characterization of ti4aln3, Metallurgical and Materials Transactions A 31 (2000) 333–337. doi:10.1007/s11661-000-0268-y.

[4] M. W. Barsoum, T. El-Raghy, The max phases: Unique new carbide and nitride materials: Ternary ceramics turn out to be surprisingly soft and machinable, yet also heat-tolerant, strong and lightweight, American Scientist 89 (2001) 334–343.

[5] M. Naguib, V. N. Mochalin, M. W. Barsoum, Y. Gogotsi, 25th anniversary article: Mxenes: a new family of two-dimensional materials, Advanced Materials 26 (2014) 992–1005. doi:10.1002/adma.201304138.

[6] M. Khazaei, A. Ranjbar, M. Arai, T. Sasaki, S. Yunoki, Electronic properties and applications of mxenes: a theoretical review, Journal of Materials Chemistry C 5 (2017) 2488–2503. doi:10.1039/C7TC00140A.

[7] Y. Gogotsi, Q. Huang, Mxenes: two-dimensional building blocks for future materials and devices, ACS Nano 15 (2021) 5775–5780. doi:10.1021/acsnano.1c03161.

[8] B. Anasori, Y. Gogotsi, 2D metal carbides and nitrides (MXenes), volume 416, Springer, 2019.

[9] M. Khazaei, M. Arai, T. Sasaki, C.-Y. Chung, N. S. Venkataramanan, M. Estili, Y. Sakka, Y. Kawazoe, Novel electronic and magnetic properties of two-dimensional transition metal carbides and nitrides, Advanced Functional Materials 23 (2013) 2185–2192. doi:10.1002/adfm.201202502.

[10] D. Er, J. Li, M. Naguib, Y. Gogotsi, V. B. Shenoy, Ti3c2 mxene as a high capacity electrode material for metal (li, na, k, ca) ion batteries, ACS Applied Materials & Interfaces 6 (2014) 11173–11179. doi:10.1021/am501144q.

[11] B. Anasori, M. R. Lukatskaya, Y. Gogotsi, 2d metal carbides and nitrides (mxenes) for energy storage, Nature Reviews Materials 2 (2017) 1–17. doi:10.1038/natrevmats.2016.98.

[12] A. Ostadhossein, J. Guo, F. Simeski, M. Ihme, Functionalization of 2d materials for enhancing oer/orr catalytic activity in li-oxygen batteries, Communications Chemistry 2 (2019) 1–11. doi:10.1038/s42004-019-0196-2.

[13] O. Mashtalir, K. M. Cook, V. N. Mochalin, M. Crowe, M. W. Barsoum, Y. Gogotsi, Dye adsorption and decomposition on two-dimensional titanium carbide in aqueous media, Journal of Materials Chemistry A 2 (2014) 14334–14338. doi:10.1039/C4TA02638A.

[14] Z. Guo, J. Zhou, L. Zhu, Z. Sun, Mxene: a promising photocatalyst for water splitting, Journal of Materials Chemistry A 4 (2016) 11446–11452. doi:10.1039/C6TA04414J.

[15] A. Tariq, S. I. Ali, D. Akinwande, S. Rizwan, Efficient visible-light photocatalysis of 2d-mxene nanohybrids with gd3+-and sn4+-codoped bismuth ferrite, ACS Omega 3 (2018) 13828–13836. doi:10.1021/acsomega.8b01951.

[16] P. Kuang, J. Low, B. Cheng, J. Yu, J. Fan, Mxene-based photocatalysts, Journal of Materials Science & Technology 56 (2020) 18–44. doi:10.1016/j.jmst.2020.02.037.

[17] X. Li, Y. Bai, X. Shi, N. Su, G. Nie, R. Zhang, H. Nie, L. Ye, Applications of mxene (ti3c2tx) in photocatalysis: A review, Materials Advances 2 (2021) 1570–1594. doi:10.1039/D0MA00938E.

[18] C. E. Ren, K. B. Hatzell, M. Alhabeb, Z. Ling, K. A. Mahmoud, Y. Gogotsi, Charge- and size-selective ion sieving through ti3c2tx mxene membranes, The Journal of Physical Chemistry Letters 6 (2015) 4026–4031. doi:10.1021/acs.jpclett.5b01895.

[19] J. Chen, K. Chen, D. Tong, Y. Huang, J. Zhang, J. Xue, Q. Huang, T. Chen, Co2 and temperature dual responsive "smart" mxene phases, Chemical Communications 51 (2015) 314–317. doi:10.1039/C4CC07220K.

[20] P. Khakbaz, M. Moshayedi, S. Hajian, M. Soleimani, B. B. Narakathu, B. J. Bazuin, M. Pourfath, M. Z. Atashbar, Titanium carbide mxene as nh3 sensor: realistic first-principles study, The Journal of Physical Chemistry C 123 (2019) 29794–29803. doi:10.1021/acs.jpcc.9b09823.

[21] A. D. Dillon, M. J. Ghidiu, A. L. Krick, J. Griggs, S. J. May, Y. Gogotsi, M. W. Barsoum, A. T. Fafarman, Highly conductive optical quality solution-processed films of 2d titanium carbide, Advanced Functional Materials 26 (2016) 4162–4168. doi:10.1002/adfm.201600357.

[22] N. Driscoll, A. G. Richardson, K. Maleski, B. Anasori, O. Adewole, P. Lelyukh, L. Escobedo, D. K. Cullen, T. H. Lucas, Y. Gogotsi, F. Vitale, Two-dimensional ti3c2 mxene for high-resolution neural interfaces, Acs Nano 12 (2018) 10419–10429. doi:10.1021/acsnano.8b06014.

[23] Y. Dong, S. Chertopalov, K. Maleski, B. Anasori, L. Hu, S. Bhattacharya, A. M. Rao, Y. Gogotsi, V. N. Mochalin, R. Podila, Saturable absorption in 2d ti3c2 mxene thin films for passive photonic diodes, Advanced Materials 30 (2018) 1705714. doi:10.1002/adma.201705714.

[24] P. Salles, D. Pinto, K. Hantanasirisakul, K. Maleski, C. E. Shuck, Y. Gogotsi, Electrochromic effect in titanium carbide mxene thin films produced by dip-coating, Advanced Functional Materials 29 (2019) 1809223. doi:10.1002/adfm.201809223.

[25] M. Naguib, O. Mashtalir, J. Carle, V. Presser, J. Lu, L. Hultman, Y. Gogotsi, M. W. Barsoum, Two-dimensional transition metal carbides, ACS Nano 6 (2012) 1322–1331. doi:10.1021/nn204153h.

[26] J.-C. Lei, X. Zhang, Z. Zhou, Recent advances in mxene: Preparation, properties, and applications, Frontiers of Physics 10 (2015) 276–286. doi:10.1007/s11467-015-0493-x.

[27] K. Huang, Z. Li, J. Lin, G. Han, P. Huang, Two-dimensional transition metal carbides and nitrides (mxenes) for biomedical applications, Chemical Society Reviews 47 (2018) 5109–5124. doi:10.1039/C7CS00838D.

[28] M. Long, H. J. Rack, Titanium alloys in total joint replacement-a materials science perspective, Biomaterials 19 (1998) 1621–1639. doi:10.1016/S0142-9612(97)00146-4.

[29] J. D. Gouveia, G. Novell-Leruth, F. Viñes, F. Illas, J. R. B. Gomes, The ti2co2 mxene as a nucleobase 2d sensor: A first-principles study, Applied Surface Science 544 (2021) 148946. doi:10.1016/j.apsusc.2021.148946.

[30] B. Xu, M. Zhu, W. Zhang, X. Zhen, Z. Pei, Q. Xue, C. Zhi, P. Shi, Ultrathin mxene-micropattern-based field-effect transistor for probing neural activity, Advanced Materials 28 (2016) 3333–3339. doi:10.1002/adma.201504657.

[31] L. Wu, X. Lu, Dhanjai, Z.-S. Wu, Y. Dong, X. Wang, S. Zheng, J. Chen, 2d transition metal carbide mxene as a robust biosensing platform for enzyme immobilization and ultrasensitive detection of phenol, Biosensors and Bioelectronics 107 (2018) 69–75. doi:10.1016/j.bios.2018.02.021.

[32] C. Chen, M. Boota, P. Urbankowski, B. Anasori, L. Miao, J. Jiang, Y. Gogotsi, Effect of glycine functionalization of 2d titanium carbide (mxene) on charge storage, Journal of Materials Chemistry A 6 (2018) 4617–4622. doi:10.1039/C7TA11347A.

[33] R. B. Rakhi, P. Nayak, C. Xia, H. N. Alshareef, Novel amperometric glucose biosensor based on mxene nanocomposite, Scientific Reports 6 (2016) 1–10. doi:10.1038/srep36422.

[34] H. Lin, Y. Chen, J. Shi, Insights into 2d mxenes for versatile biomedical applications: current advances and challenges ahead, Advanced Science 5 (2018) 1800518. doi:10.1002/advs.201800518.

[35] D. F. Sharman, The catabolism of catecholamines: recent studies, British Medical Bulletin 29 (1973) 110–115. doi:10.1093/oxfordjournals.bmb.a070978.

[36] M. A. Piggott, E. F. Marshall, N. Thomas, S. Lloyd, J. A. Court, E. Jaros, D. Burn, M. Johnson, R. H. Perry, I. G. McKeith, C. Ballard, E. K. Perry, Striatal dopaminergic markers in dementia with lewy bodies, alzheimer's and parkinson's diseases: rostrocaudal distribution, Brain 122 (1999) 1449–1468. doi:10.1093/brain/122.8.1449.

[37] Y. Lei, D. Butler, M. C. Lucking, F. Zhang, T. Xia, K. Fujisawa, T. Granzier-Nakajima, R. Cruz-Silva, M. Endo, H. Terrones, M. Terrones, A. Ebrahimi, Single-atom doping of mos2 with manganese enables ultrasensitive detection of dopamine: Experimental and computational approach, Science Advances 6 (2020) eabc4250. doi:10.1126/sciadv.abc425.

[38] C. W. Berridge, D. M. Devilbiss, Psychostimulants as cognitive enhancers: the prefrontal cortex, catecholamines, and attention-deficit/hyperactivity disorder, Biological Psychiatry 69 (2011) e101–e111. doi:10.1016/j.biopsych.2010.06.023.

[39] Wikipedia contributors, Serine — Wikipedia, the free encyclopedia, https://en.wikipedia.org/w/index.php?title=Serine&oldid=1101734383, 2022. [Online; accessed 1-October-2022].

[40] P. E. Blöchl, Projector augmented-wave method, Physical Review B 50 (1994) 17953. doi:10.1103/PhysRevB.50.17953.

[41] G. Kresse, D. Joubert, From ultrasoft pseudopotentials to the projector augmented-wave method, Physical Review B 59 (1999) 1758. doi:10.1103/PhysRevB.59.1758.

[42] J. P. Perdew, K. Burke, M. Ernzerhof, Generalized gradient approximation made simple, Physical Review Letters 77 (1996) 3865. doi:10.1103/PhysRevLett.77.3865.

[43] G. Kresse, J. Furthmüller, Efficiency of ab-initio total energy calculations for metals and semiconductors using a plane-wave basis set, Computational Materials Science 6 (1996) 15–50. doi:10.1016/0927-0256(96)00008-0.

[44] G. Kresse, J. Furthmüller, Efficient iterative schemes for ab initio total-energy calculations using a plane-wave basis set, Physical Review B 54 (1996) 11169. doi:10.1103/PhysRevB.54.11169.

[45] S. Grimme, Semiempirical gga-type density functional constructed with a long-range dispersion correction, Journal of Computational Chemistry 27 (2006) 1787–1799. doi:10.1002/jcc.20495.

[46] H. J. Monkhorst, J. D. Pack, Special points for brillouin-zone integrations, Physical Review B 13 (1976) 5188. doi:10.1103/PhysRevB.13.5188.

[47] C. G. Broyden, The convergence of a class of double-rank minimization algorithms 1. general considerations, IMA Journal of Applied Mathematics 6 (1970) 76–90. doi:10.1093/imamat/6.1.76.

[48] C. G. Broyden, The convergence of a class of double-rank minimization algorithms: 2. the new algorithm, IMA Journal of Applied Mathematics 6 (1970) 222–231. doi:10.1093/imamat/6.3.222.

[49] J. Heyd, G. E. Scuseria, M. Ernzerhof, Hybrid functionals based on a screened coulomb potential, The Journal of Chemical Physics 118 (2003) 8207–8215. doi:10.1063/1.1564060.

[50] G. Henkelman, A. Arnaldsson, H. Jónsson, A fast and robust algorithm for bader decomposition of charge density, Computational Materials Science 36 (2006) 354–360. doi:10.1016/j.commatsci.2005.04.010.

[51] K. Momma, F. Izumi, Vesta 3 for three-dimensional visualization of crystal, volumetric and morphology data, Journal of Applied Crystallography 44 (2011) 1272–1276. doi:10.1107/S0021889811038970.

[52] A. Togo, I. Tanaka, First principles phonon calculations in materials science, Scripta Materialia 108 (2015) 1–5. doi:10.1016/j.scriptamat.2015.07.021.

[53] S. Kajiyama, L. Szabova, K. Sodeyama, H. Iinuma, R. Morita, K. Gotoh, Y. Tateyama, M. Okubo, A. Yamada, Sodium-ion intercalation mechanism in mxene nanosheets, ACS Nano 10 (2016) 3334–3341. doi:10.1021/acsnano.5b06958.

[54] C. Kittel, P. McEuen, Introduction to solid state physics, John Wiley & Sons, 2018.

[55] ???? See Supplemental Material at [URL will be inserted by publisher] for the phonon dispersion spectra calculated without and with Hubbard parameter, the AFM and FM configurations along with their structural parameters of Ti_3C_2 monolayer, brief explanation of why these molecules

were chosen for this study, as well as electronic properties of Ti_3C_2+M, $Ti_3C_2(OH)_2$+M and Ti_3C_2+M with Ti-vacancy systems.

[56] I. R. Shein, A. L. Ivanovskii, Graphene-like titanium carbides and nitrides tin+1cn, tin+1nn (n=1, 2, and 3) from de-intercalated max phases: First-principles probing of their structural, electronic properties and relative stability, Computational Materials Science 65 (2012) 104–114. doi:10.1016/j.commatsci.2012.07.011.

[57] Z. H. Fu, Q. F. Zhang, D. Legut, C. Si, T. C. Germann, T. Lookman, S. Y. Du, J. S. Francisco, R. F. Zhang, Stabilization and strengthening effects of functional groups in two-dimensional titanium carbide, Physical Review B 94 (2016) 104103. doi:10.1103/PhysRevB.94.104103.

[58] I. R. Shein, A. L. Ivanovskii, Planar nano-block structures tin+1al0.5cn and tin+1cn (n= 1, and 2) from max phases: Structural, electronic properties and relative stability from first principles calculations, Superlattices and Microstructures 52 (2012) 147–157. doi:10.1016/j.spmi.2012.04.014.

[59] K. C. Berridge, T. E. Robinson, J. W. Aldridge, Dissecting components of reward:'liking','wanting', and 'learning', Current Opinion in Pharmacology 9 (2009) 65–73. doi:10.1016/j.coph.2008.12.014.

[60] M. N. Baliki, A. Mansour, A. T. Baria, L. Huang, S. E. Berger, H. L. Fields, A. V. Apkarian, Parceling human accumbens into putative core and shell dissociates encoding of values for reward and pain, Journal of Neuroscience 33 (2013) 16383–16393. doi:10.1523/JNEUROSCI.1731-13.2013.

[61] J. M. Wenzel, N. A. Rauscher, J. F. Cheer, E. B. Oleson, A role for phasic dopamine release within the nucleus accumbens in encoding aversion: a review of the neurochemical literature, ACS Chemical Neuroscience 6 (2015) 16–26. doi:10.1021/cn500255p.

[62] S. Puglisi-Allegra, R. Ventura, Prefrontal/accumbal catecholamine system processes high motivational salience, Frontiers in Behavioral Neuroscience 6 (2012) 31. doi:10.3389/fnbeh.2012.00031.

[63] J. Moncrieff, The myth of the chemical cure, Springer, 2008.

[64] N. D. Volkow, G.-J. Wang, S. H. Kollins, T. L. Wigal, J. H. Newcorn, F. Telang, J. S. Fowler, W. Zhu, J. Logan, Y. Ma, K. Pradhan, C. Wong, J. M. Swanson, Evaluating dopamine reward pathway in adhd: clinical implications, JAMA 302 (2009) 1084–1091. doi:10.1001/jama.2009.1308.

[65] H.-P. Zhang, X.-Y. Lin, X. Lu, Z. Wang, L. Fang, Y. Tang, Understanding the interfacial interactions between dopamine and different graphenes for biomedical materials, Materials Chemistry Frontiers 1 (2017) 1156–1164. doi:10.1039/C6QM00300A.

[66] M. Ghasemi, F. Rezania, J. Lewin, K. P. Moore, A. R. Mani, d-serine modulates neurogenic relaxation in rat corpus cavernosum, Biochemical Pharmacology 79 (2010) 1791–1796. doi:10.1016/j.bcp.2010.02.007.

[67] M. Mozafari, M. Soroush, Surface functionalization of mxenes, Materials Advances 2 (2021) 7277–7307. doi:10.1039/D1MA00625H.

[68] Z.-H. Chen, Z.-N. Zhang, H.-Q. Zhang, D. Hu, Z.-B. Ye, Y. Zhang, Y. Yu, B.-H. Nie, H.-X. Xi, C.-X. Duan, Modification of ti3c2 mxene nanosheets with tunable properties using a post-processing method, Rare Metals 41 (2022) 3100–3106. doi:10.1007/s12598-022-02017-x.

[69] H. Riazi, S. K. Nemani, M. C. Grady, B. Anasori, M. Soroush, Ti3c2 mxene-polymer nanocomposites and their applications, Journal of Materials Chemistry A 9 (2021) 8051–8098. doi:10.1039/D0TA08023C.

[70] T. A. Manz, N. G. Limas, Introducing ddec6 atomic population analysis: Part 1. charge partitioning theory and methodology, RSC Advances 6 (2016) 47771–47801. doi:10.1039/C6RA04656H.

[71] N. G. Limas, T. A. Manz, Introducing ddec6 atomic population analysis: Part 2. computed results for a wide range of periodic and nonperiodic materials, RSC Advances 6 (2016) 45727–45747. doi:10.1039/C6RA05507A.

[72] T. A. Manz, Introducing ddec6 atomic population analysis: Part 3. comprehensive method to compute bond orders, RSC Advances 7 (2017) 45552–45581. doi:10.1039/C7RA07400J.

[73] T.-C. Leung, C. L. Kao, W. S. Su, Y. J. Feng, C. T. Chan, Relationship between surface dipole, work function and charge transfer: Some exceptions to an established rule, Physical Review B 68 (2003) 195408. doi:10.1103/PhysRevB.68.195408.

[74] A. M. Sampaio, J. F. R. V. Silveira, L. G. Dias, J. L. F. D. Silva, L. J. A. Siqueira, Adsorption of ionic liquids forming species on ti3c2tx mxenes surfaces by first-principle calculations, FlatChem 35 (2022) 100413. doi:10.1016/j.flatc.2022.100413.

[75] Y. Wang, Y. Li, L. Tang, J. Lu, J. Li, Application of graphene-modified electrode for selective detection of dopamine, Electrochemistry Communications 11 (2009) 889–892. doi:10.1016/j.elecom.2009.02.013.

[76] C. Zhu, S. Guo, Y. Fang, S. Dong, Reducing sugar: new functional molecules for the green synthesis of graphene nanosheets, ACS Nano 4 (2010) 2429–2437. doi:10.1021/nn1002387.

[77] W. Cui, M. Li, J. Liu, B. Wang, C. Zhang, L. Jiang, Q. Cheng, A strong integrated strength and toughness artificial nacre based on dopamine cross-linked graphene oxide, ACS Nano 8 (2014) 9511–9517. doi:10.1021/nn503755c.

[78] J. D. Gouveia, G. Novell-Leruth, P. M. L. S. Reis, F. Viñes, F. Illas, J. R. B. Gomes, First-principles calculations on the adsorption behavior of amino acids on a titanium carbide mxene, ACS Applied Bio Materials 3 (2020) 5913–5921. doi:10.1021/acsabm.0c00621.

[79] N. M. Tran, Q. T. H. Ta, A. Sreedhar, J.-S. Noh, Ti3c2tx mxene playing as a strong methylene blue adsorbent in wastewater, Applied Surface Science 537 (2021) 148006. doi:10.1016/j.apsusc.2020.148006.

[80] I. Ozdemir, A. W. Holleitner, C. Kastl, O. Ü. Aktürk, Thickness and defect dependent electronic, optical and thermoelectric features of wte2, Scientific Reports 12 (2022) 1–16. doi:10.1038/s41598-022-16899-5.

[81] Z. Lin, B. R. Carvalho, E. Kahn, R. Lv, R. Rao, H. Terrones, M. A. Pimenta, M. Terrones, Defect engineering of two-dimensional transition metal dichalcogenides, 2D Materials 3 (2016) 022002. doi:10.1088/2053-1583/3/2/022002.

[82] J. A. Robinson, B. Schuler, Engineering and probing atomic quantum defects in 2d semiconductors: A perspective, Applied Physics Letters 119 (2021) 140501. doi:10.1063/5.0065185.

Supplementary Material: Exploring the Adsorption Mechanisms of Neurotransmitter and Amino Acid on Ti_3C_2-MXene Monolayer: Insights from DFT Calculations

Ilkay Ozdemir[a,b], Handan Arkin[c], Milorad V. Milošević[b], Johannes V. Barth[d], Ethem Aktürk[a,d,*]

[a]*Physics Department, Adnan Menderes University, Aydın, 09100, Turkey*
[b]*Department of Physics, University of Antwerp, Groenenborgerlaan 171, B-2020, Antwerp, Belgium*
[c]*Department of Physics Engineering, Faculty of Engineering, Ankara University, Tandogan, Ankara, 06100, Turkey*
[d]*Physics Department E20, Technical University of Munich (TUM), James Franck Strasse1, 85748, Garching, Munich, Germany*

Abstract

In this study, we conducted a systematic density functional theory (DFT) investigation of the interaction between Ti_3C_2-MXene monolayer and biological molecules dopamine (DA) and serine (Ser) as neurotransmitter and amino acid, respectively. Our calculations show good agreement with previous literature findings for the optimized Ti_3C_2 monolayer. We found that DA and Ser molecules bind to the Ti_3C_2 surface with adsorption energies of $-2.244\,\mathrm{eV}$ and $-3.960\,\mathrm{eV}$, respectively. The adsorption of Ser resulted in the dissociation of one H atom. Electronic density of states analyses revealed little changes in the electronic properties of the Ti_3C_2-MXene monolayer upon adsorption of the biomolecules. We further investigated the interaction of DA and Ser with Ti_3C_2 monolayers featuring surface-termination with OH functional group, and Ti-vacancy. Our calculations indicate that the adsorption energies significantly decrease in the presence of surface termination, with adsorption energies of $-0.097\,\mathrm{eV}$ and $-0.330\,\mathrm{eV}$ for DA and Ser, respectively. Adsorption energies on the Ti-vacancy surface, on the other hand, are cal-

*Corresponding author
Email address: ethem.akturk@adu.edu.tr (Ethem Aktürk)

culated to be −3.584 eV and −3.856 eV for DA and Ser, respectively. Our results provide insights into the adsorption behavior of biological molecules on Ti_3C_2-MXene, demonstrating the potential of this material for biosensing and other biomedical applications. These findings highlight the importance of surface modifications in the development of functional materials and devices based on Ti_3C_2-MXene, and pave the way for future investigations into the use of 2D materials for biomedical applications.

Keywords: MXene, 2D Materials, Density Functional Theory (DFT), Dopamine, Serine, Biosensing, Biomedical Applications

---

1. Stability of Ti_3C_2 Monolayer

In this section, we present the stability analysis of Ti_3C_2 monolayer in terms of phonon dispersion curves calculated without (w/o) and with (w) Hubbard parameter (see Fig.S1). Positive phonon frequencies verify the stability and are in very well agreement with literature findings [1].

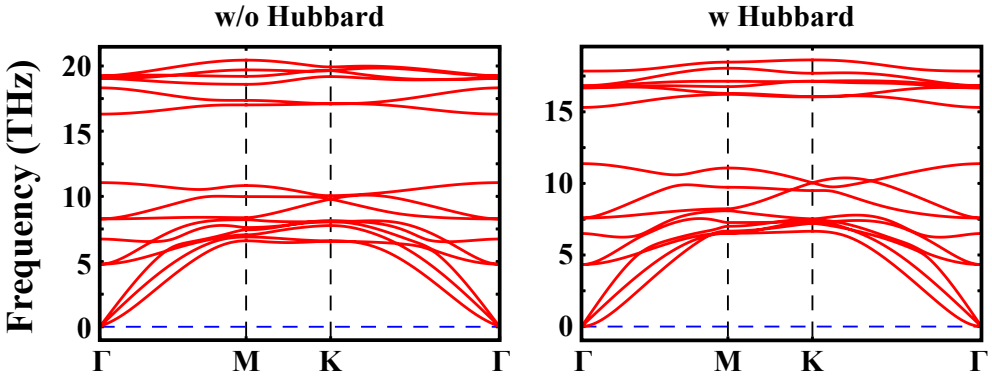

Figure S1: Phonon dispersion curves calculated both without (w/o) and with (w) the Hubbard parameter, along the main symmetry directions of the Brillouin zone, for Ti_3C_2 monolayer.

2. Magnetic Configurations Considered for Ti_3C_2 Monolayer

In this section, we present the calculated magnetic configurations, including anti-ferromagnetic (AFM) and ferromagnetic (FM) spin-orientations, without the Hubbard parameter for the Ti_3C_2 monolayer (see Fig.S2). As

shown in the figure, the AFM configuration has a lower energy, and we calculated a difference of 0.037 eV/unitcell between the two configurations (which is reported as 0.043 eV/unitcell in the study by Fu et al. [4]). Therefore, it is reasonable to conclude that the AFM state is the ground state of Ti_3C_2, consistent with previous findings in the literature [2, 3, 4]. We also provide a comparison of the structural parameters calculated for AFM and FM states in Table S1, along with relevant parameters reported in the literature for the sake of comparison.

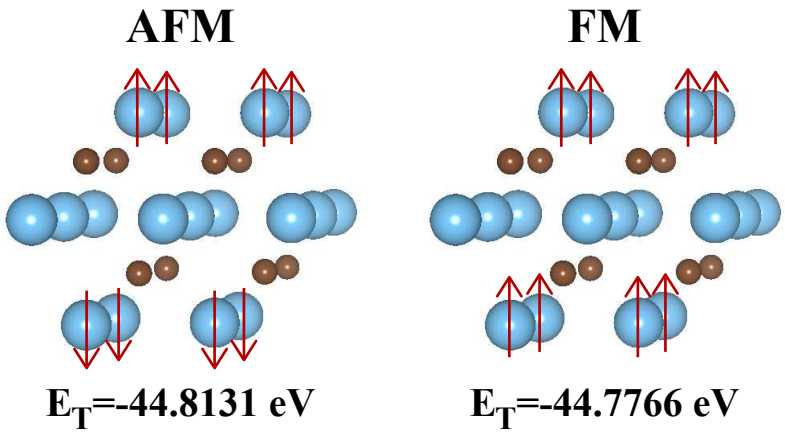

Figure S2: Comparison of anti-ferromagnetic (AFM) and ferromagnetic (FM) spin alignments for Ti_3C_2 monolayer. Here, the red arrows indicate the direction of spin orientations of the corresponding atoms. Ti atoms in the intermediate layer and C atoms are nonmagnetic.

Table S1: Calculated structural parameters without Hubbard parameter for antiferromagnetic (AFM) and ferromagnetic (FM) orders of Ti_3C_2 monolayer, and literature findings for some of them: The lattice constants, in the (xy)-plane $\mid \vec{a} \mid = \mid \vec{b} \mid$=a, and along z direction (vacuum), $\mid \vec{c} \mid$=c; the thickness parameter, Δz; the bond lengths between neighboring Ti and C atoms, d_1 (Ti(1)-C(1) and Ti(2)-C(2)), d_2 (Ti(3)-C(1) and Ti(3)-C(2)); cohesive energy per atom, E_{coh}; the average electronic charge transfer from Ti atoms to C atoms according to Bader charge analysis; magnetic moment in the unit cell and per Ti atom, μ_B.

Study	lattice constants		thickness parameter	bond lengths		cohesive energy	charge transfer	magnetic moment μ (μ_B)	
	a (Å)	c (Å)	Δz (Å)	d_1 (Å)	d_2 (Å)	E_{coh} (eV/atom)	$\Delta\rho$ (e)	unit cell	on Ti
				AFM					
present	3.097	20	4.677	2.067	2.212	6.98	1.16	–	0.76
Ref.-[3]	3.085	–	4.742	2.083	–	6.82	–	–	0.74
Ref.-[4]	–	–	–	2.065	2.214	–	1.18	–	0.75
				FM					
present	3.098	20	4.674	2.064	2.214	6.97	1.17	1.79	0.62
Ref.-[1]	3.098	18.96	–	2.048	2.221	–	–	–	–
Ref.-[5]	–	–	–	2.064	–	–	–	1.93	–

3. Selected Molecules

In this section, we present our findings, obtained through first-principles based density functional theory (DFT) calculations, regarding the selected biological molecules in the scope of this study, along with their literature comparisons. As indicated in the main text, we selected dopamine (DA) as neurotransmitter molecule and serine (Ser) as amino acid.

We present bond lengths and energy levels calculated for the selected biological molecules in Fig.S3, which are in well agreement with experimental/theoretical data [6, 7, 8, 9].

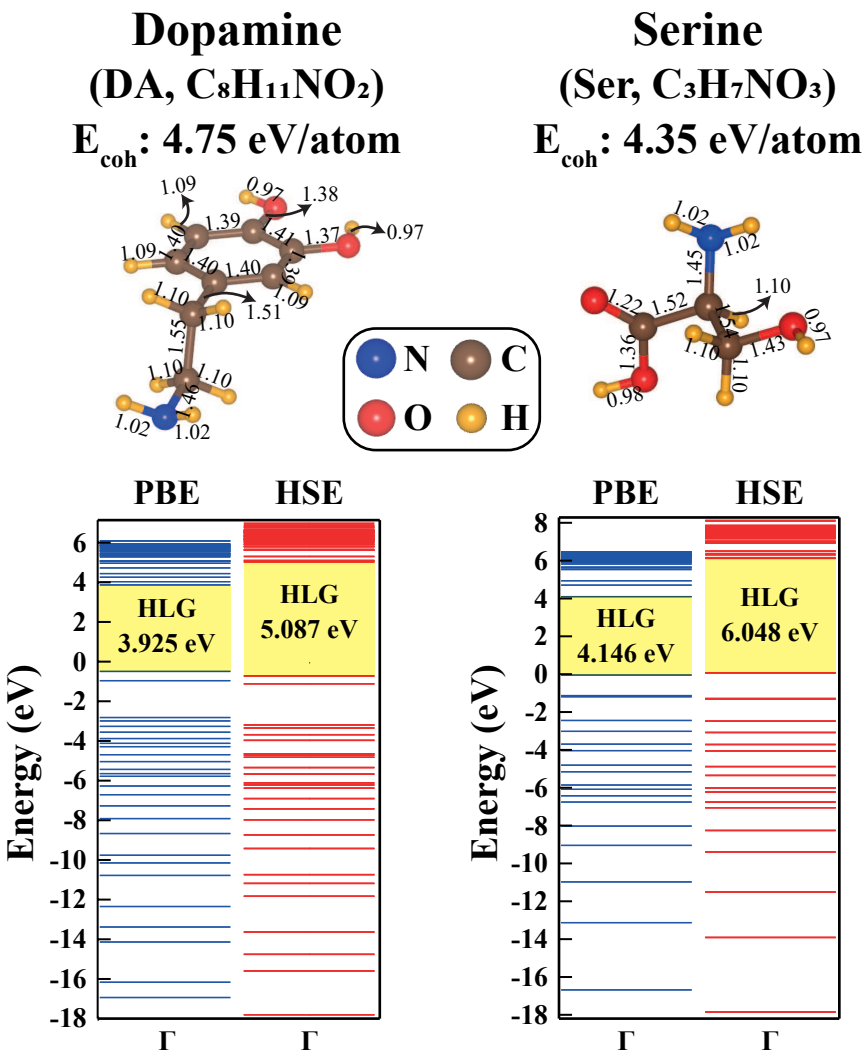

Figure S3: Optimized atomic structures with calculated bond lengths, and electronic energy diagrams calculated by PBE and HSE06 for the selected biological molecules. The HOMO-LUMO energy gap (HLG) corresponding to each molecule is presented by yellow-shaded area and its numerical value is given inset. Cohesive energy (E_{coh}) values calculated per atom are also indicated.

4. Electronic Properties of Ti_3C_2+M (M:DA,Ser) Systems

In this section, we present the isosurfaces of electronic charge density difference, $\Delta\rho(\mathbf{r})$, which is obtained by subtracting the charge densities situated at the Ti_3C_2 substrate and molecule sites from the charge density of total system, and electronic density of states (DOS) graphs calculated for Ti_3C_2+DA and Ti_3C_2+Ser (see Fig.S4).

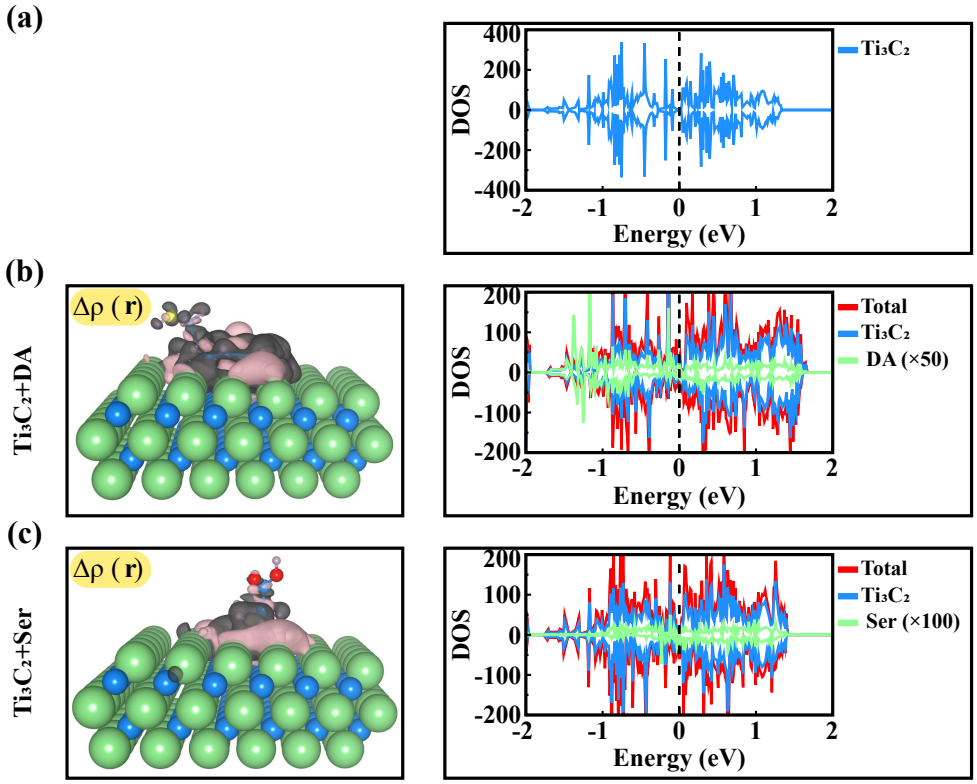

Figure S4: Isosurfaces of electronic charge density difference, $\Delta\rho(\mathbf{r})$, and total and partial electronic density of states calculated for **(a)** pristine (6×6) super cell of Ti_3C_2 monolayer, **(b)** Ti_3C_2+DA and **(c)** Ti_3C_2+Ser systems. Pink and black isosurfaces respectively indicate positive and negative charge regions. The isosurfaces are set to $0.0008\,e/Å^3$. In the DOS graphs, Fermi energy is set to zero and indicated by black-dashed lines.

5. Electronic Properties of $Ti_3C_2(OH)_2$+M (M:DA,Ser) Systems

In this section, we present the isosurfaces of electronic charge density difference, $\Delta\rho(\mathbf{r})$, which is obtained by subtracting the charge densities situated at the $Ti_3C_2(OH)_2$ substrate and molecule sites from the charge density of total system, and electronic density of states (DOS) graphs calculated for $Ti_3C_2(OH)_2$+DA and $Ti_3C_2(OH)_2$+Ser (see Fig.S5).

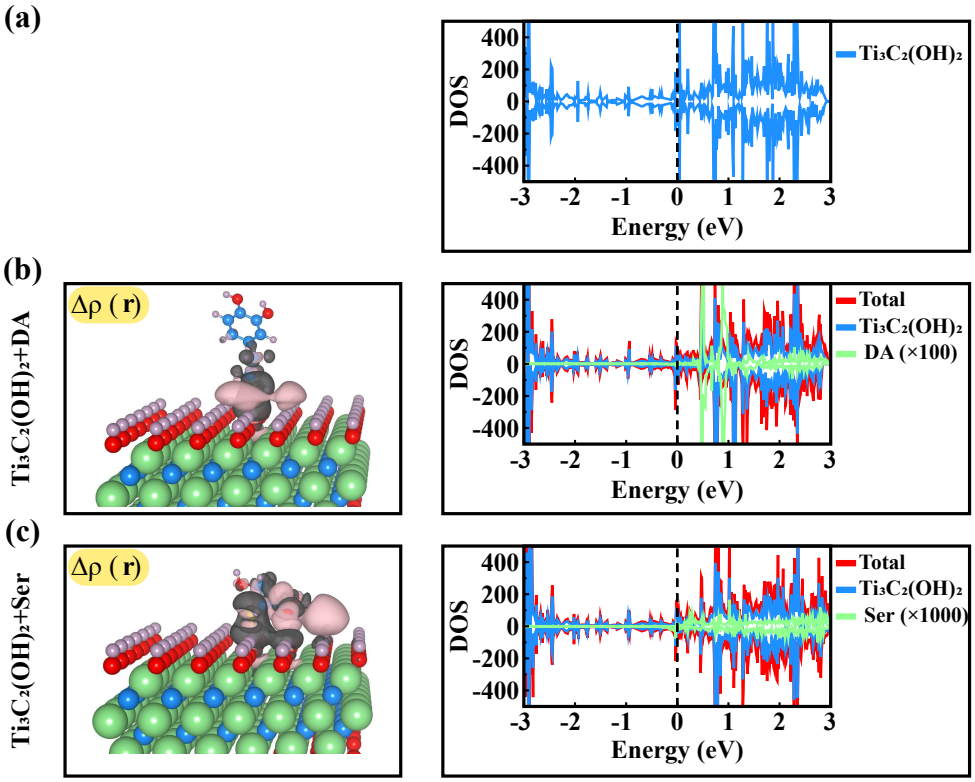

Figure S5: Isosurfaces of electronic charge density difference, $\Delta\rho(\mathbf{r})$, and total and partial electronic density of states calculated for **(a)** pristine (6×6) super cell of $Ti_3C_2(OH)_2$ monolayer, **(b)** $Ti_3C_2(OH)_2$+DA and **(c)** $Ti_3C_2(OH)_2$+Ser systems. Pink and black isosurfaces respectively indicate positive and negative charge regions. The isosurfaces are set to 0.0003 e/Å^3. In the DOS graphs, Fermi energy is set to zero and indicated by black-dashed lines.

6. Electronic Properties of Ti-vacancy Ti_3C_2+M (M:DA,Ser) Systems

In this section, we present the isosurfaces of electronic charge density difference, $\Delta\rho(\mathbf{r})$, which is obtained by subtracting the charge densities situated at the Ti_3C_2 substrate with Ti-vacancy defect and molecule sites from the charge density of total system, and electronic density of states (DOS) graphs calculated for Ti-vacancy Ti_3C_2+DA and Ti_3C_2+Ser (see Fig.S6).

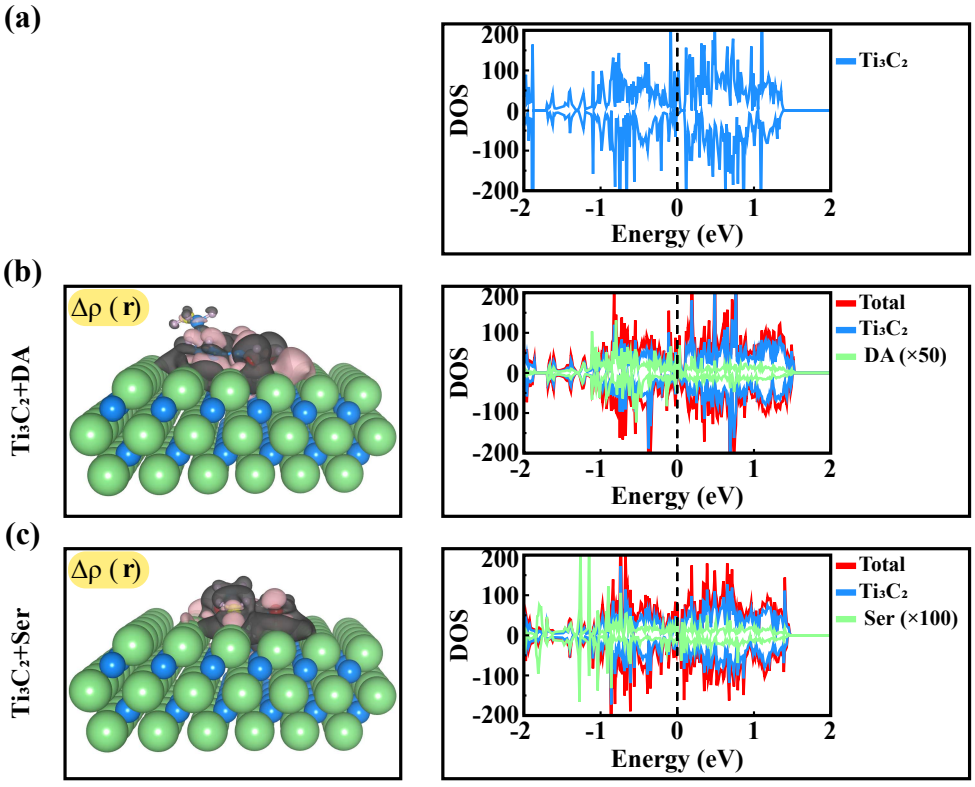

Figure S6: Isosurfaces of electronic charge density difference, $\Delta\rho(\mathbf{r})$, and total and partial electronic density of states calculated for **(a)** Ti-vacancy pristine Ti_3C_2, **(b)** Ti_3C_2+DA and **(c)** Ti_3C_2+Ser systems. Pink and black isosurfaces respectively indicate positive and negative charge regions. The isosurfaces are set to $0.0012\,e/Å^3$. In the DOS graphs, Fermi energy is set to zero and indicated by black-dashed lines.

7. Work Function of Ti_3C_2+M (M:DA,Ser) Systems

In this section, we present the work fucntion values calculated using Equation(4) in the main text, and corresponding plots for Ti_3C_2+M (M:DA, Ser) systems. As can be seen from the Fig.S7, the work fucntion values on the top and bottom surfaces. This is because the bottom and top surfaces are not identical: one is clean, and the other has corresponding molecules adsorbed on it. Since the system has a net dipole moment, which in turn changes the quantitative value of work function.

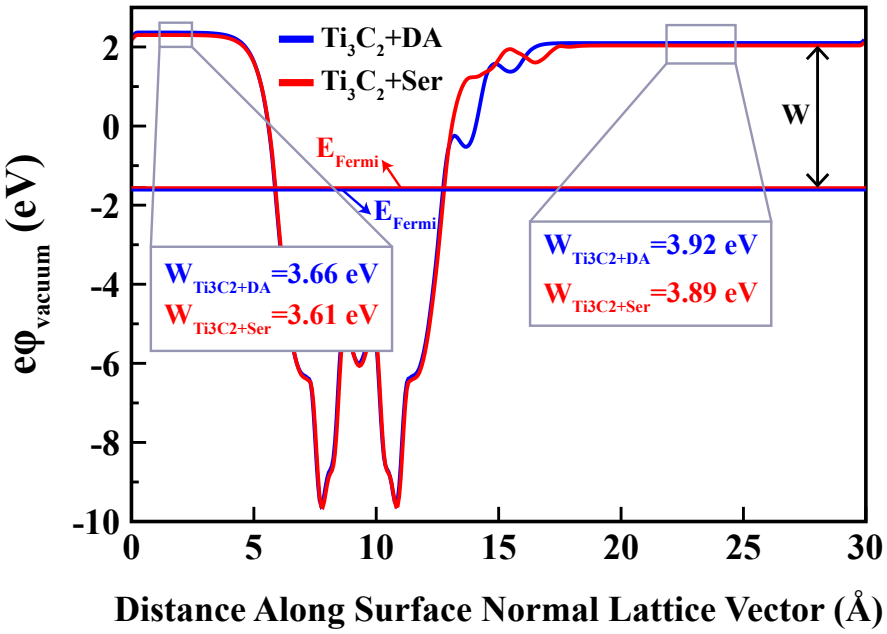

Figure S7: Determination of work function by comparing the Fermi level with the local Coulombic potential in the vacuum for Ti_3C_2+M (M:DA, Ser) systems.

8. Acknowledgments

This work is supported by TUBITAK under Project No. 118F508. IO thanks to the Council of Higher Education (the CoHE) 100/2000 Program and to the Scientific and Technological Research Council of Turkey (TUBITAK) BIDEB-2214/A Program for providing doctoral scholarships. E. A. acknowledges the Alexander von Humboldt Foundation for a Research Fellowship for Experienced Researchers. The computational resources are provided by TÜBITAK ULAKBIM, High Performance and Grid Computing Center (TR-Grid e-Infrastructure), the Leibniz Supercomputing Centre.

References

[1] T. Hu, J. Wang, H. Zhang, Z. Li, M. Hu, and X. Wang, *Vibrational properties of Ti_3C_2 and $Ti_3C_2T_2$ (T = O, F, OH) monosheets by first-principles calculations: a comparative study*, Phys. Chem. Chem. Phys. **17**, 9997 (2015).

[2] I. R. Shein, and A. L. Ivanovskii, *Planar nano-block structures $Ti_{n+1}Al_{0.5}C_n$ and $Ti_{n+1}C_n$ (n = 1, and 2) from MAX phases: Structural, electronic properties and relative stability from first principles calculations*, Superlattices and microstructures **52**, 147 (2012).

[3] I. R. Shein, and A. L. Ivanovskii, *Graphene-like titanium carbides and nitrides $Ti_{n+1}C_n$, $Ti_{n+1}N_n$ (n = 1, 2, and 3) from de-intercalated MAX phases: First-principles probing of their structural, electronic properties and relative stability*, Comput. Mater. Sci. **65**, 104 (2012).

[4] Z. H. Fu, Q. F. Zhang, D. Legut, C. Si, T. C. Germann, T. Lookman, S. Y. Du, J. S. Francisco, and R. F. Zhang, *Stabilization and strengthening effects of functional groups in two-dimensional titanium carbide*, Phys. Rev. B **94**, 104103 (2016).

[5] Q. Tang, Z. Zhou, and P. Shen, *Are MXenes promising anode materials for Li ion batteries? Computational studies on electronic properties and Li storage capability of Ti_3C_2 and $Ti_3C_2X_2$ (X = F, OH) monolayer*, J. Am. Chem. Soc. **134**, 16909 (2012).

[6] S. S. Deshpande, D. B. Potekar, P. B. Shelke, and M. D. Deshpande, *Theoretical study of interaction of $Fe_{13}O_8$@$Zn_{48}O_48$ cluster with*

dopamine: Magnetic and optical properties, Journal of Molecular Graphics and Modelling **99**, 107640 (2020).

[7] A. C. Rossi-Fernández, L. A. Meier, and N. J. Castellani, *Neutral and zwitterionic dopamine species adsorbed on silver surfaces: A DFT investigation of interaction mechanism*, International Journal of Quantum Chemistry **119**, e25817 (2019).

[8] I. Bald, S. Weigelt, X. Ma, P. Xie, R. Subramani, M. Dong, C. Wang, W. Mamdouh, J. Wang, and F. Besenbacher, *Two-dimensional network stability of nucleobases and amino acids on graphite under ambient conditions: adenine, L-serine and L-tyrosine*, Phys. Chem. Chem. Phys. **12**, 3616 (2010).

[9] E. V. Boldyreva, E. N. Kolesnik, T. N. Drebushchak, H. Ahsbahs, J. A. Beukes, and H. P. Weber, *A comparative study of the anisotropy of lattice strain induced in the crystals of L-serine by cooling down to 100 K or by increasing pressure up to 4.4 GPa*, Z. Kristallogr. **220**, 25 (2005).